PAPER

Check for updates

Natural tea polyphenol functionalized graphene anode for simultaneous power production and degradation of methyl orange dye in microbial fuel cells†

Deliang Guo, Qikai Fu,‡ Xinru Wang, Ling Li, Xiaolin Xu ID * and Xiongfang An*

The microbial fuel cell (MFCs) has dual functions, capable of achieving dye decolorization and synchronous power generation. Despite these advantages, the MFCs have faced challenges related to low electron transfer efficiencies and limited dye treatment capacity in wastewater applications. This work introduces an innovative approach by employing reduced graphene oxide-modified carbon cloth (TP-RGO@CC) anodes, utilizing tea polyphenols as the reducing agent. This modification significantly enhances the hydrophilicity and biocompatibility of the anodes. The MFC equipped with the TP-RGO@CC anode demonstrated a remarkable increase in the maximum power density, reaching 773.9 mW m^{-2}, representing a 22% improvement over the plain carbon cloth electrode. The decolorization rate of methyl orange (50 mg L^{-1}, pH 7) reached 99% within 48 h. Biodiversity analysis revealed that the TP-RGO@CC anode selectively enriched electrogens producing and organic matter-degrading bacteria, promoting a dual mechanism of dye decolorization, degradation, and simultaneous electro-production at the anode. This work highlights advanced anode materials that excel in effective pollutant removal, energy conversion, and biomass reuse.

1. Introduction

The application and synthesis of dyestuffs generates a large amount of wastewater, which has a huge negative impact on the environment.[1] The azo bonds contained in azo dyes make their degradation difficult and toxic, making them one of the most difficult dyes to degrade.[2] Currently, the technologies used to treat azo dyes in wastewater include physicochemical (such as oxidative decolorization,[3] adsorption,[4] membrane separation[5]) and biological (such as aerobic/anaerobic treatment,[6] fungal technology,[7] algae[8]) methods. However, traditional treatment methods consume large amounts of energy or chemicals in decolorizing and degrading azo dye wastewater, leading to reduced energy utilization and potential secondary pollution in the post-treatment stage, as well as a sharp increase in treatment costs.[9] Therefore, under the double pressure, how to improve the performance of azo dye decolorization and at the same time increase the power generation efficiency is the core issue of this study. Microbial fuel cells (MFCs) are electrochemical devices that use microorganisms to decolorize and

degrade dyes while producing electricity.[10] It has been reported that the chemical energy of domestic wastewater (with a chemical oxygen demand of about 13 kJ g^{-1}) is approximately nine times the energy required for its treatment.[11] Effective recovery of this energy can significantly reduce economic costs for factories. Presently, when MFC treats wastewater, it not only generates additional electrical energy but also reduces energy consumption in the treatment process, thereby enhancing treatment efficiency and increasing added value. Consequently, this innovative technology meets the growing demand for sustainable energy and reduces environmental pollution from azo dyes.

The progress in MFC development has been remarkable, but challenges like low power output and extended startup times persist.[12] At the anode, organic matter produces electrons through microbial catalysis. The transfer of these electrons from microorganisms to the electrode surface inside the anode chamber involves two mechanisms: electron mediators (or shuttles) and nanoconductors.[13] Based on this fact, the development of anode materials capable of influencing electricity-producing microorganisms and extracellular electron transfer (EET) has far-reaching implications for MFC applications. Common carbon-based materials (such as carbon cloth and carbon felt) are popular choices for MFC electrodes due to their stability and corrosion resistance. However, these materials possess smooth and highly hydrophobic surfaces, hindering

School of Chemistry and Chemical Engineering, Key Laboratory of Environmental Monitoring and Pollutant Control, Shihezi University, Shihezi 832003, China. E-mail: xuxl@shzu.edu.cn; shz_anxiongf@163.com

† Electronic supplementary information (ESI) available. See DOI: https://doi.org/10.1039/d4ra00613e

‡ These authors contributed equally to this work.

microbial colonization and growth on the anode, coupled with poor electrical conductivity.[14] Therefore, modifying the surface of carbon-based materials to enhance hydrophilicity and electrical conductivity stands as a viable strategy to enhance the overall performance of MFC.

Due to the unique structure, reduced graphene oxide (RGO) is suitable for MFC electrode as a prominent carbon material, which has high electrical conductivity and electrochemical stability. Coupled with the large specific surface area, RGO can provide more attachment sites for microorganisms.[15] Although the antimicrobial properties of graphene have been mentioned in several studies, they are affected by the preparation method and the synergistic modification with other materials.[16] Sayed *et al.* doped GO on carbon brushes using electrophoresis and improved the electron transfer process in microorganisms by increasing the power density by more than 10 times under real wastewater conditions.[17] It is demonstrated that the electrochemical performance of MFCs can be enhanced by graphene-modified anodes.

Strong reducing chemicals (*e.g.* hydrazine, a commonly used strong reducing agent) are often used in the production of RGO, which consumes hazardous reagents and has environmental implications.[18] Tea polyphenols are mainly obtained through chemical synthesis or direct extraction from tea leaves. In comparison to chemical synthesis, the direct extraction and separation of tea polyphenols are considered more environmentally friendly and sustainable. This is because chemical synthesis frequently results in negative impacts due to the use of solvents, production of by-products, and low reaction efficiency.[19] Currently, solvents such as water and organic reagents are commonly utilized for direct extraction and separation. However, some organic solvents pose challenges in terms of recovery, toxicity, flammability, and safety hazards.[20] Therefore, the water extraction method is preferred for its environmental benefits. Green tea as a common traditional beverage in daily life is easily available. Green tea extracts contain tea polyphenol compounds, which are considered significant constituents,[21,22] are excellent reduce agents due to their ability to provide electrons or hydrogen atoms in chemical reactions. The hydroxyl and carbonyl compounds in the extract were used as hydrophilic groups to increase the hydrophilic properties of RGO.[23,24] In addition, the tea dregs as a good biomass resource, which can still extract a variety of active ingredients, processed and converted into more applicable value-added materials,[25,26] has a good economic added value. Verma *et al.* successfully reduced graphene oxide (GO) using a variety of green plant extracts, including green tea, which showed low electrical resistance in both electrochemical analyses such as Nyquist and improved electronic conductivity compared to GO, and has potential for use as an energy storage material.[27] Therefore, employing tea polyphenol-reduced GO-modified carbon cloth in MFCs is a favorable choice.

In this study, carbon cloth was used as the substrate material and modified by reducing GO using tea polyphenol. The TP-RGO@CC anode was fabricated by the solution impregnation method. This modification aimed to enhance the hydrophilicity and biocompatibility of anode, ultimately improving EET

efficiency and dye degradation performance. The changes in chemical and physical properties of different anodes were explored by micro-morphology and hydrophilicity. The electrochemical properties of the different anodes were measured and evaluated by cyclic voltammetry and electrochemical impedance spectroscopy. In addition, the ability of MFCs with different anodes to decolorize and degrade methyl orange under various conditions was assessed by monitoring the variation in methyl orange concentration in the anode chamber. The microbial community composition on the surface of the modified carriers was analyzed using high-throughput sequencing, elucidating the role of the modified anode in microbial community succession and the mechanism of performance enhancement. This study presents a green and effective anode preparation method for the efficient degradation of methyl orange wastewater using MFCs.

2. Materials and methods

2.1. Chemicals and inoculums

Carbon cloth (CC, W0S1009) was bought from CeTech Co., Ltd (Shanghai, China). Carbon felt with thickness 3 mm was obtained from Hot-Material Co., Ltd, China. Green tea was purchased from Lipton Green Tea Co., Ltd, China. Graphite powder were purchased from Shanghai Macklin Biochemical Co., Ltd. Anaerobic sludge from Shihezi Second Wastewater Treatment Plant (Shihezi, China) was used as the inoculum strain.

2.2. Preparation of green tea extract

2 g of green tea powder was added to 40 g of deionized water, sonicated for 30 min, and then heated in a water bath at 85 °C for 40 min. The impurities were removed by filtration and the filtrate was retained as tea polyphenol extract (TP, Texts 1, 2, Fig. S1†).

2.3. Electrodes preparation

The treated carbon cloth electrodes were used as plain CC. GO was prepared from graphite powder using a modified Hummers' method.[28] Then, 100 mg of GO was dispersed into 100 mL of deionized water and sonicated for 30 min to obtain a stable yellow-brown solution (100 mg/100 mL). After that, RGO was prepared by adding 2 mL of ammonia solution water and stirring for 8 h in a 90 °C water bath. Finally, the pretreated carbon cloths were separately soaked in RGO solution for 10 h and dried at 60 °C until constant weight to obtain RGO@CC anode.

For TP-RGO–CC electrode: tea polyphenol-reduced graphene oxide (TP-RGO) was prepared by adding 10 mL of TP extract solution to the above GO dispersion and stirring for 8 h in a 90 °C water bath. Similarly, carbon cloth was soaked in TP-RGO solution and dried to obtain TP-RGO@CC anode.

2.4. MFC construction and operation

The MFC was constructed using a two-chamber device (Fig. S2,† Wenoote Co., Ltd) with a single chamber volume of 100 mL,

using a Nafion 117 proton exchange membrane to separate the microbial fuel cell into two polar chambers, using a batch operation mode in a 30 ± 1 °C thermostat. The anodes were TP-RGO@CC, RGO@CC, or plain CC. The cathode used a 4 cm carbon felt (thickness 3 mm, Hot-Material Co., Ltd, China) of the same size. Fresh anode culture solution was used in the anode chamber: 1.0 g L^{-1} sodium acetate, 50 mM phosphate buffer solution (PBS, 0.31 g L^{-1} NH_4Cl, 0.13 g L^{-1} KCl, 2.45 g L^{-1} NaH_2PO_4, 4.58 g L^{-1} Na_2HPO_4, pH 6.8–6.9), 5 mL L^{-1} vitamin solution (Table S2†) and 12.5 mL L^{-1} trace element solution (Table S3†).[29,30] A 30% (v/v) sludge suspension was used as the starting stock solution, which was removed when the voltage reached its peak and remained stable. The cathode electrolyte was a mixture of 50 mM $K_3[Fe(CN)_6]$ and 50 mM PBS buffer solution. Unless otherwise stated, all MFCs were operated with an external resistive (1000 Ω) load.

2.5. Material characterisation

The surface morphologies of electrodes were observed through scanning electron microscopy (SEM, Zeiss Merlin Compact). The X-ray diffraction (XRD, Rigaku SmartLab 9 kW) patterns were obtained by testing GO, RGO@CC, and TP-RGO@CC anode. The Fourier transform infrared (FTIR, TENSOR II, Bruker) spectra were utilized to test the functional groups of the GO, RGO@CC, TP-RGO@CC, and TP extract solutions. Raman spectra were obtained on a Raman spectrometer (LabRam HR Evolution) with a He–Ne laser (632.8 nm) as excitation source. The hydrophilic property of each anode was measured by a contact angle system (DSA100, Kruss, Germany).

2.6. Electrochemical analysis

The output voltage of the MFC was collected and recorded every 30 min at intervals using an online data acquisition system (Modbus M2001, Smacq Co., Ltd, China) for the cell voltage data points. After stable operation, the external resistance was varied in the range of 10 000–50 Ω. The reactor was operated at each resistance value until the voltage stabilized, the voltage and current at the corresponding resistance values were recorded. The current and power density were normalized to the projected area of the anode for analysis to obtain the polarization and power density curves.

Electrochemical performance measurements, specifically cyclic voltammetry (CV) and electrochemical impedance spectroscopy (EIS), were conducted using an electrochemical workstation (CHI760E, CH Instruments, Inc.) featuring a three-electrode system: the cell anode as the working electrode, a platinum wire (CH Instruments, Inc.) as the counter electrode, and an Ag/AgCl electrode (CH Instruments, Inc.) as the reference electrode. The CV graph was obtained within a scan range of −0.4 to 1.0 V, at a scan rate of 10 mV s^{-1}. EIS measurements covered a frequency range of 100 000 to 0.01 Hz.

The change in chemical oxygen demand (COD) of the anode effluent is measured using the standard potassium dichromate method.[31] The coulombic efficiency (CE), which measures the conversion efficiency of chemical energy into electrical energy, is calculated as the ratio of the actual charge produced by the MFC to the theoretical charge produced.

2.7. Degradation of methyl orange dye

In the methyl orange degradation experiments, methyl orange solution was introduced to the anode electrolyte. After a stable operation period of 400 h, various concentrations of methyl orange solution (50, 100, 200 mg L^{-1}) were incorporated into the anode solution, operating under different pH conditions (5, 7, 9). Subsequently, the spectrophotometer measured the methyl orange concentration in the anode solution at 465 nm.[32] Upon completion of the operation, the anode biofilm was collected and sent to Yanqu Information Technology Co., Ltd (Hangzhou, China). The 16S V3–V4 region was amplified through polymerase chain reaction (PCR) to establish the biofilm library, which underwent high-throughput sequencing. Furthermore, QIIME was employed for data analysis, and statistical tests and data visualization were conducted using the R language. Lastly, the amount of flora on 0.5 cm × 1 cm anode was assessed using the bicinchoninic acid (BCA) protein assay.

3. Results and discussion

3.1. Properties of the material

The preparation process scheme is depicted in Fig. 1a. In brief, the TP extract is dispersed in a GO solution. In the course of the reaction, TP reduces GO, altering its structure. Following this, the carbon cloth is immersed in the solution mentioned above and then dried to yield TP-RGO@CC. Fig. 1b–g displays SEM images of different electrodes. The carbon fibers on the surface of the blank carbon cloth skeleton (Fig. 1b and e) were neatly arranged and smooth, with almost no impurities on the surface. After the modification, RGO@CC (Fig. 1c and f) exhibited a rough surface, demonstrate the effective alteration of the carbon cloth surface with RGO. As illustrated in Fig. 1d and g, the comparative analysis with RGO@CC revealed that the surface of TP-RGO@CC exhibited a more extensive coverage with RGO lamellae. This enhancement could be attributed to the addition of TP, which mitigated agglomeration during the reduction process, leading to a more uniform attachment of RGO on the carbon cloth surface.[33] The rough surface morphology provides additional attachment sites for microorganisms, fostering the formation and growth of biofilms at the anode, as noted in previous research. The increased microbial presence is considered a crucial factor contributing to the improvement of EET efficiency in MFC.

For GO materials, the reduction process implies a reduction of the oxide groups in the structure. In the XRD test (Fig. 2a), the 2θ angle characteristic diffraction peak of GO was 11°. After the reduction by ammonia or TP, the diffraction peaks changed and the 2θ angle shifted to 20.3° and 23.6°, respectively, proving that the reduction reaction occurred in both systems. In addition, the diffraction peaks of the TP-RGO@CC anode became broad and short, suggesting irregular doping in the material and a reduction in RGO toxicity, promoting microorganism growth.[34] The FTIR spectra characterized the types of functional
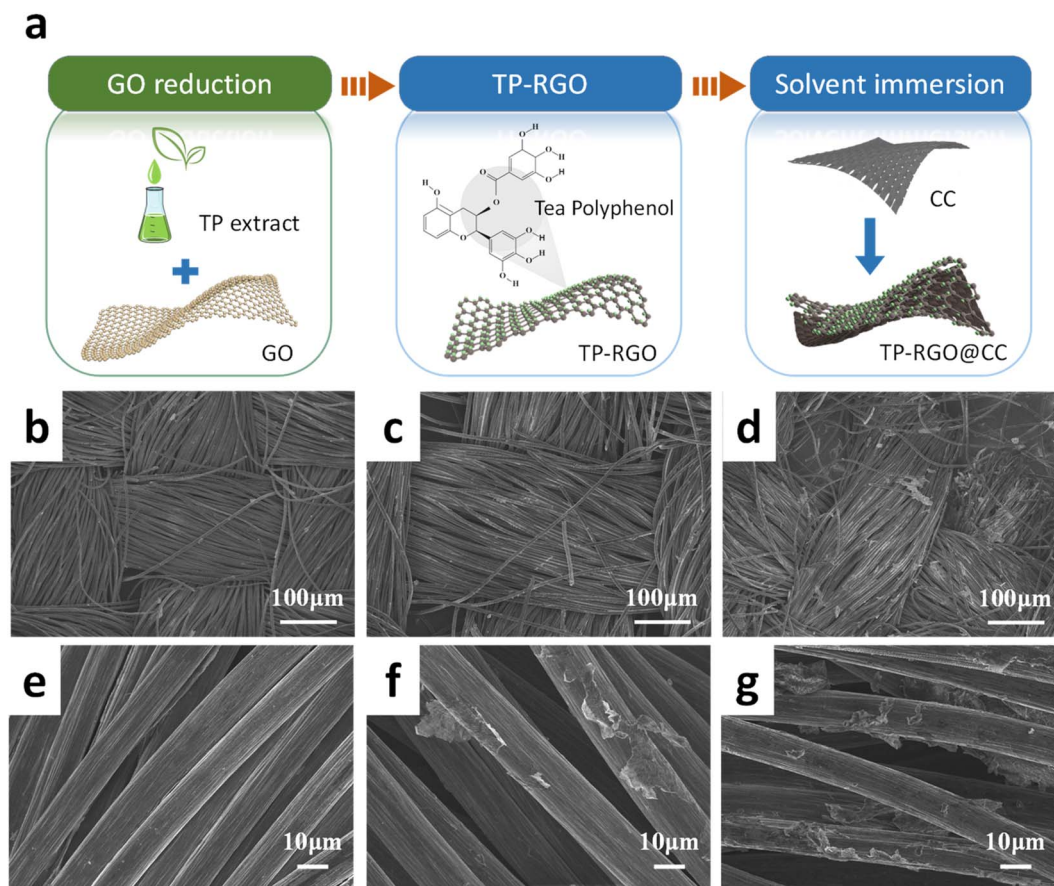
Fig. 1 (a) Schematic illustration for preparation of the TP-RGO@CC anode; SEM images of anodes (b) and (e) CC; (c) and (f) RGO@CC; (d) and (g) TP-RGO@CC.

groups contained in GO, RGO@CC, TP-RGO@CC and TP extract (Fig. 2b). The O–H oscillatory peaks of GO and the C=O stretching peaks of aromatic groups are located at about 3432 cm^{-1} and 1730 cm^{-1}, respectively. However, these oxygen-containing functional groups are significantly weakened in the RGO@CC and TP-RGO@CC anodes after the reduction reaction. In the RGO@CC samples, the N–H stretching vibrational peaks of the amide group and C–N group appear at 1556 cm^{-1} and 1409 cm^{-1}, respectively, indicating the dominance of ammonia in the reduction of GO. Additionally, the binding of biomolecules to TP-RGO@CC produces spectra similar to those of TP extracts. Notably, the peaks of the TP-RGO@CC anode at 1649 cm^{-1} and 1155 cm^{-1} are attributed to tea polyphenols in the TP extract.[35] This implies that TP promote GO reduction and indicate the binding of biomolecules with RGO in TP-RGO@CC anode.

The electrodes made from RGO material were examined using Raman spectra. The peaks of G and D bands, around 1596 and 1345 cm^{-1} respectively in Fig. 2c, indicate structural differences in the materials. The carbon atoms in GO exhibit a disordered arrangement ($I_D/I_G = 1.11$). The modified RGO@CC anode shows a distinct C–C sp^2 bond G resonance characteristic peak. Additionally, the I_D/I_G ratios for RGO@CC and TP-RGO@CC were 0.89 and 1.05, respectively. Notably, TP-

RGO@CC has a higher I_D/I_G intensity ratio compared to RGO@CC, suggesting the presence of narrowed sp^2 structural domains during plant-mediated GO bioreduction. The carbon–oxygen bonding functional groups in the TP increase the extent of structural defects, providing specific surface polarity and conductive properties to the conjugated carbon skeleton. This offers additional active sites for bacteria.

The surface hydrophilicity of the electrode plays a crucial role in determining the extent of binding of electroactive microorganisms, subsequently influencing the efficiency of electricity production in MFC. The water contact angle on the electrode surface is depicted in Fig. 2d. The ordinary carbon cloth exhibited strong hydrophobicity with a water contact angle of 139.1 ± 2.4°. The hydrophilicity of the RGO@CC electrode surface was moderately enhanced, as evidenced by a reduced water contact angle to 124.9 ± 3.1°. These results indicate that the use of RGO-modified electrodes can effectively improve the hydrophilicity of the electrode. The water contact angle of TP-RGO@CC is significantly reduced to 31.5 ± 1.2°. Compared to plain carbon cloth, it decreased by about 41%, and compared to RGO, it went down by 33%. The incorporation of biomolecules enhances the hydrophilicity of the electrode, fostering the colonization and growth of microorganisms on the electrode surface. This facilitates the adhesion of more
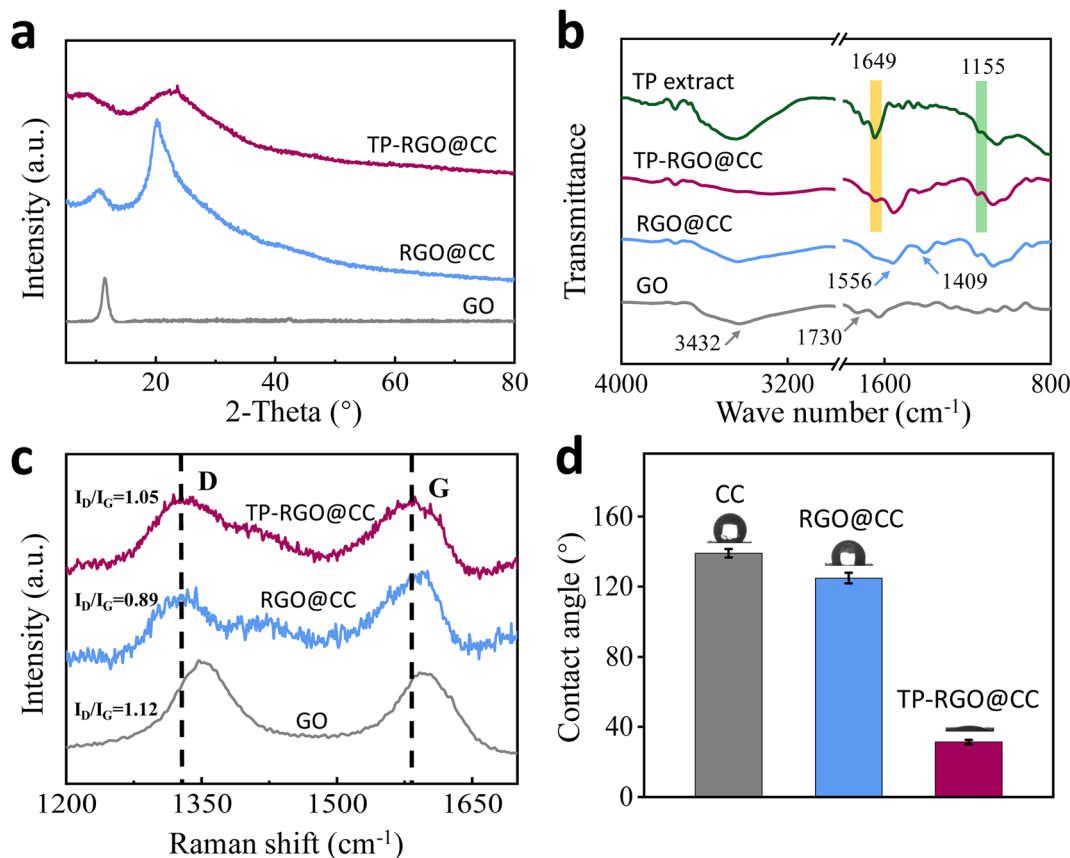
Fig. 2 (a) XRD spectra; (b) FTIR spectra; (c) Raman spectra and (d) contact angles of CC, RGO@CC, TP-RGO@CC anodes.

electrochemically active bacteria to the electrode, potentially improving EET efficiency.

3.2. Electrochemical properties of different anodes

In cyclic voltammetry testing of the material, differences in redox peaks were observed among the various electrodes (Fig. 3a), indicating variances in the electrochemical activities of the electrodes. The addition of RGO notably enhanced the redox peaks in RGO@CC, highlighting the exceptional conductivity of RGO materials and its positive impact electrochemical reactivity of the electrodes. Among the electrodes, TP-RGO@CC exhibited the most significant peak current and achieved the largest redox peak area, showcasing superior electrochemical performance. These findings underscore that surface modification effectively increases the number of electrochemically active sites on the electrodes. This improvement enhances the capacity to accept bacterial electrons, resulting in a reduction of interfacial charge transfer resistance and facilitating interfacial electron transfer.

After the MFC was started, the biofilm formed due to the growth and colonization of microorganisms on the anode surface causes changes in the electrochemical properties of the anode. CV tests were performed on the MFC during the same cycle of voltage output stabilization (Fig. 3b). The normal CC electrode exhibited the lowest peak redox value. Following modification, the peak current (1.39 mA) of the RGO@CC electrode significantly increased. This enhancement could be

attributed to the RGO@CC anode promoting a stronger binding between microorganisms and the electrode. For the TP-RGO@CC anode, two significant redox peaks were observed at potentials −0.33 V (anode) and −0.14 V (cathode) and 0.08 V (anode) and 0.52 V (cathode), respectively. It was hypothesized that these two sets of redox peaks might be due to *MtrC* in the c-type outer membrane pigment proteins, as well as direct electron transfer generated by bacterially secreted electron shuttles.[36] Additionally, the increased electrochemical activity of the electrodes facilitated efficient electron transfer, thus showcasing unique electrochemical properties.

The electrode resistance was analyzed using electrochemical impedance spectroscopy (EIS), and Fig. 3c showed the Nyquist plots for different anodes, and the ohmic resistance R_s and charge transfer resistance R_{ct} obtained by fitting the data using ZView (Table S4†). The different anodes exhibit similar ohmic resistances (R_s). The plain CC anode shows high electron transfer resistance (235.4 Ω). The RGO significantly decreases the charge transfer resistance (R_{ct}) of the modified RGO@CC electrode (49.5 Ω) due to its excellent electrical conductivity. The MFC with the TP-RGO@CC anode demonstrates an R_{ct} of 14.6 Ω, indicating a certain increase in electron transfer capacity. The TP-RGO@CC anode exhibited reduced electron transfer resistance due to enhanced microbial attachment, promoting a tight binding of bacteria to the electrode surface.[37] This green
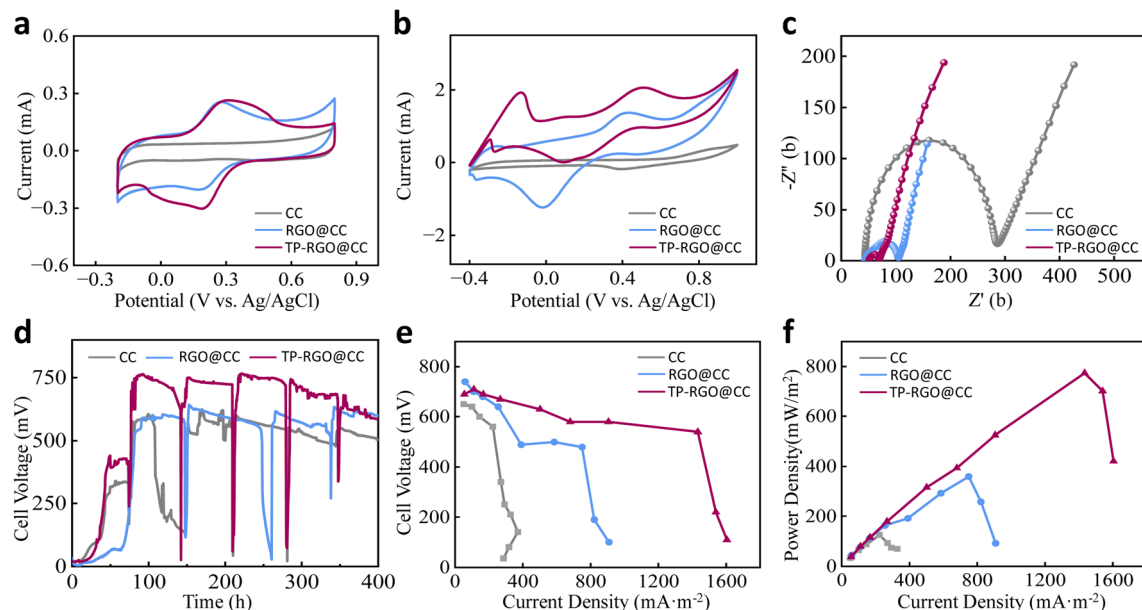
Fig. 3 (a) The cyclic voltammetry curve CV of the material was scanned in PBS solution; (b) the CV curve of the material in MFCs; (c) Nyquist plots of different anodes; (d) time course of voltage output; (e) and (f) the polarization and power density curves as a function of the current density of MFCs with different anodes.

RGO anode effectively reduces charge transfer resistance and enhancing the EET efficiency of MFC.

The continuous voltage–time profile for the 400 h is depicted in Fig. 3d. The MFC equipped with TP-RGO@CC completed startup at 48 h, demonstrate enhanced bacterial activity that reduced the startup time. Achieving a maximum stabilized voltage of approximately 750 mV after 60 h, being about 1.3 times that of the plain CC electrode. Furthermore, the MFC with the RGO@CC anode reached a maximum output voltage of about 642 mV, compared to the CC anode (603 mV). This demonstrates that RGO modification has a beneficial impact power generation capability in the MFC, enabling more efficient electron collection in the anode and accelerating electron transfer. Meanwhile, the TP-RGO@CC anode obtained the highest operating voltage, with each cycle duration significantly shorter than that of the other two groups. This indicates that microorganisms on the electrode can rapidly decompose organic matter in the MFC, reflecting superior microbial activity.

Fig. 3e and f illustrate the polarization and power density curves. The high resistance of CC anode results in a steeper slope of the MFC polarization curve. After the modification, the slope of MFC polarization curve running on RGO@CC is reduced. It can be attributed to the fact that RGO has excellent electrical conductivity, which effectively reduces the internal resistance of the MFC. Meanwhile, a maximum power density of 359.7 mW m^{-2} is obtained for RGO@CC. Operating the MFC with the TP-RGO@CC anode increased the power density to a maximum of 773.9 mW m^{-2}. The use of a natural extract as a reducing agent minimized the toxicity of material and facilitated bacteria binding to the electrode. Simultaneously, the RGO modification increased the specific surface area of the

carbon cloth, providing more loading area for microorganisms and significantly improving the power generation capacity of MFC. Polarization curves obtained by running the TP-RGO@CC anode displayed a minimum slope and an open-circuit voltage of 690 mV. The RGO modification enhanced the electrochemical activity of anode, resulting in a maximum power density 6.2 times higher than that of plain CC (124.8 mW m^{-2}). The power density was enhanced by 41.2% compared to MFCs using reduced graphene oxide metal nanoparticle anodes in other studies.[38] These results suggest that the TP-RGO@CC anode demonstrates superior electrochemical performance, thereby making a significant contribution to the power generation of the MFC. Moreover, the use of fewer organic reagents in material preparation contributed to a more efficient and environmentally friendly green chemical process.

3.3. Dye degradation properties of MFC

In the experiments investigating the decolorization and degradation of dyes by MFC, the influence of concentration and pH on the degradation process was examined. In Fig. 4a, the COD degradation rate of MFCs operating different anodes at three concentrations is illustrated. It is evident that the COD degradation rate for all three electrodes decreased to varying degrees with increasing concentration, indicating that the degradation performance of MFC is affected by the concentration of the dye. The decline in COD degradation rates can be attributed to the toxic effects of high dye concentrations, resulting in a reduction in bacterial activity on the anode. Consequently, this weakens the ability to decompose organic matter anode chamber of MFC. At a concentration of 50 mg L^{-1}, the MFC with the TP-RGO@CC anode achieved an 86% COD degradation, highlighting its robust dye degradation capability. However, when
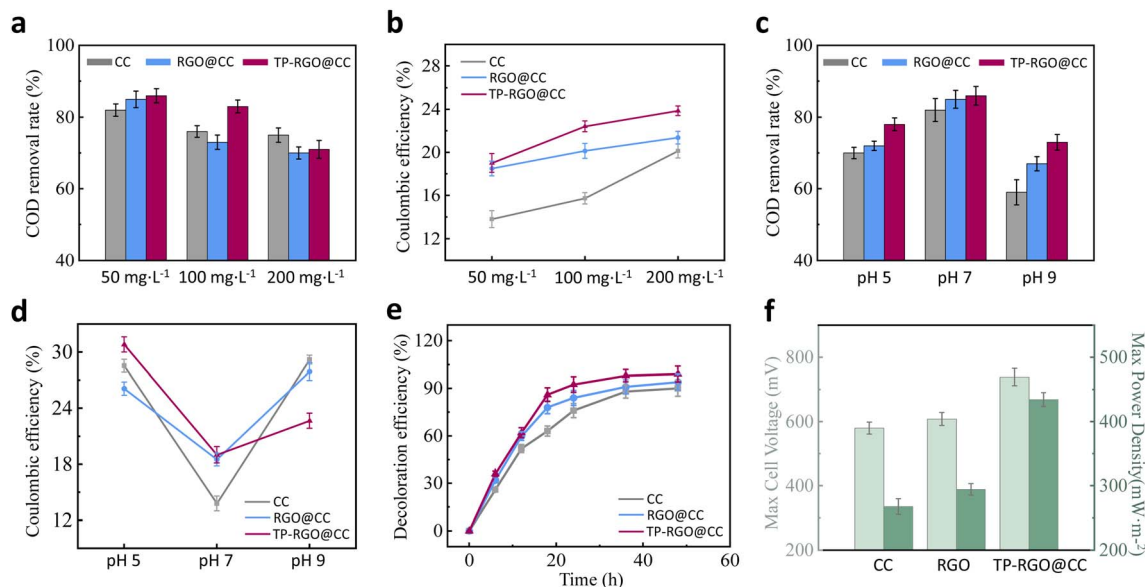
Fig. 4   (a) COD degradation rate of different anodes at different concentrations; (b) coulombic efficiency of different electrodes at different concentrations; (c) COD degradation rate of different anodes at different pH; (d) coulombic efficiency of different electrodes at different pH; (e) decolorization efficiency *versus* time at 50 mg L^{-1}, pH 7; (f) the maximum power density and max cell voltage of MFCs is closely related to the amount of biomass.

the concentration of methyl orange in the anode solution was raised to 200 mg L^{-1}, the COD degradation rate for the TP-RGO@CC anode was less affected than that for the RGO@CC anode. This observation suggests that the TP-RGO@CC anode exhibits better resilience to environmental changes and greater stability, making it a more effective choice in resisting variations in dye concentration.

In Fig. 4b, the coulomb efficiency is depicted through distinctive curves for each type of anode. The plain CC anode exhibited the lowest coulomb efficiency, indicative of its inferior electron collection capability. After modification, the exceptional electrical conductivity of RGO promotes electron transfer, thereby enhancing the electron recovery efficiency of the RGO@CC anode in the MFC. Notably, the MFC equipped with the TP-RGO@CC anode achieved the highest coulombic efficiency, reaching 23.9% at a concentration of 200 mg L^{-1}. This outcome underscores the superior electron collection ability and EET efficiency of the TP-RGO@CC anode. The presence of a diverse microbial community on the TP-RGO@CC anode further stimulated the conversion of organic matter, contributing to reduced substrate loss and consequently higher coulomb efficiency for the MFC.

The COD degradation rates under different pH conditions are presented in Fig. 4c. It is significant that MFC running three different anodes achieved the highest COD degradation rate under neutral conditions. Additionally, even under acidic conditions (pH 5), the MFC equipped with the TP-RGO@CC anode maintained a high degradation efficiency of 78%. This observation suggests that the microbial community on the anode may have relatively better adaptability to acidic conditions compared to alkaline conditions (pH 9). Particularly, the

TP-RGO@CC anode demonstrated resilience against acidic shocks to some extent.

Fig. 4d illustrates the coulomb efficiencies under different pH conditions. The MFCs running various electrodes demonstrated a substantial increase in coulomb efficiency under both acidic and alkaline conditions. This enhancement may be attributed to the elevated presence of ions in the anode solution, facilitating the rapid transfer of electrons across the anode surface. In an alkaline environment, the coulombic efficiency of the TP-RGO@CC anode was significantly lower than that of the CC and RGO@CC anodes, indicating its poorer electron collection ability under alkaline conditions. This observation underscores potential limitations of TP-RGO@CC anodes in alkaline environments.

The decolorization rate of methyl orange at 50 mg L^{-1}, pH 7, over time is presented in Fig. 4e. The CC anode exhibited a gradual stabilization and slowdown in the decolorization rate, reaching 90% after 48 h. In contrast, the RGO@CC anode underwent rapid degradation by 18 h, achieving 94% decolorization by 48 h, showcasing the effective facilitation of organic decomposition through RGO modification. Notably, the TP-RGO@CC anode reached a 92% decolorization rate at 24 h. Subsequently, the decolorization rate gradually slowed down, ultimately achieving a final decolorization rate of 99% at 48 h. This suggests that the microbial community on the TP-RGO@CC anode has the ability to rapidly decompose organic matter, providing excellent dye treatment for the MFC. Compared to conventional bacterial treatment of methyl orange azo dye,[39] it offers a significant advantage in achieving rapid and efficient degradation, particularly at higher dye concentrations. Moreover, when compared with reactors utilizing electro Fenton process,[40] the treatment process using MFC resulted in

reduced energy consumption and an increased decolorization rate by 4% at similar dye concentrations. These findings underscore the promising potential of employing MFC with TP-RGO@CC anode for various applications in environmental protection and sustainable development.

Fig. 4f illustrates the synchronized maximum voltage and power density obtained in the methyl orange decolorization experiments of the MFC. The plain CC electrode achieved a maximum power density of 267.47 mW m^{-2} and a maximum voltage of 579.61 mV. In particular, the MFC equipped with the RGO@CC anode exhibited a significantly higher power density of 294.29 mW m^{-2}. In the case of the TP-RGO@CC MFC, the power density reached 434.34 mW m^{-2}, accompanied by a maximum voltage of 738.6 mV, indicating its excellent synchronized power generation performance in dye decolorization. Concentration and pH conditions were examined in this work, but there may be other factors influencing energy production and efficiency in MFC equipped with TP-RGO@CC anode, such as temperature. Further exploration of these factors could be conducted in subsequent studies.

3.4. Bacterial morphology and abundance

After operating the MFC, the microbial loading on different anodes changed significantly under electron microscopy (Fig. 5a–c), indicating variations in the biocompatibility of the materials. The surface of the CC was smoother and had the least microbial loading, while the number of microorganisms increased to a certain extent and grew in clusters and morphological aggregated on the RGO@CC electrode surface. It could be clearly seen that the TP-RGO@CC grew extensively on carbon cloth fibers with a large number of interconnected filaments. The formation of nanoconductors between different

genera of electrogenic microorganisms was an important reason for the increased efficiency of EET. The amount of biomass in the anode biofilm was further measured by a BCA protein assay (Fig. 5d). The biomass for TP-RGO@CC was estimated as 479.3 ± 2.9 μg cm^{-2}, which was considerably higher than those of the CC (135.8 ± 1.3 μg cm^{-2}), RGO@CC (264.0 ± 1.5 μg cm^{-2}), respectively. The TP-RGO@CC anode is biocompatible and promotes the growth of microorganisms on the electrode, thereby enhancing the power production of the MFC. This is consistent with the electrochemical capabilities in the MFC performance tests described above.

The bacterial distribution on the anode surface appeared to vary significantly with the change in running time (Fig. S3†). After 1 day of MFCs operation, a small amount of bacterial attachment was observed on the surface of the three different anodes, leading to limited power production during the initial startup stages. After 3 days of operation, the RGO@CC and TP-RGO@CC anodes began to exhibit an increase in bacterial attachment due to differences in the state of the anode surfaces. This phenomenon facilitated a rapid increase in voltage during the startup phase. After 7 days of operation, dense bacterial attachment was observed on the carbon cloth fibers of TP-RGO@CC anode. This phenomenon may be promoted by the excellent biocompatibility of the TP-RGO@CC anode. The morphology of the bacteria at different stages confirms that the MFC equipped with the TP-RGO@CC anode can indeed have a stronger power production capacity. To further observe the activity of microorganisms on the anode surface at different operational stages, the anodes at 1, 3, 7, and 14 days were sampled. The bacterial distribution of active bacteria was then observed by CLSM (Fig. S4†). The green and red fluorescence intensity in the captured CLSM images was also quantified and counted by the software. It was observed that bacterial
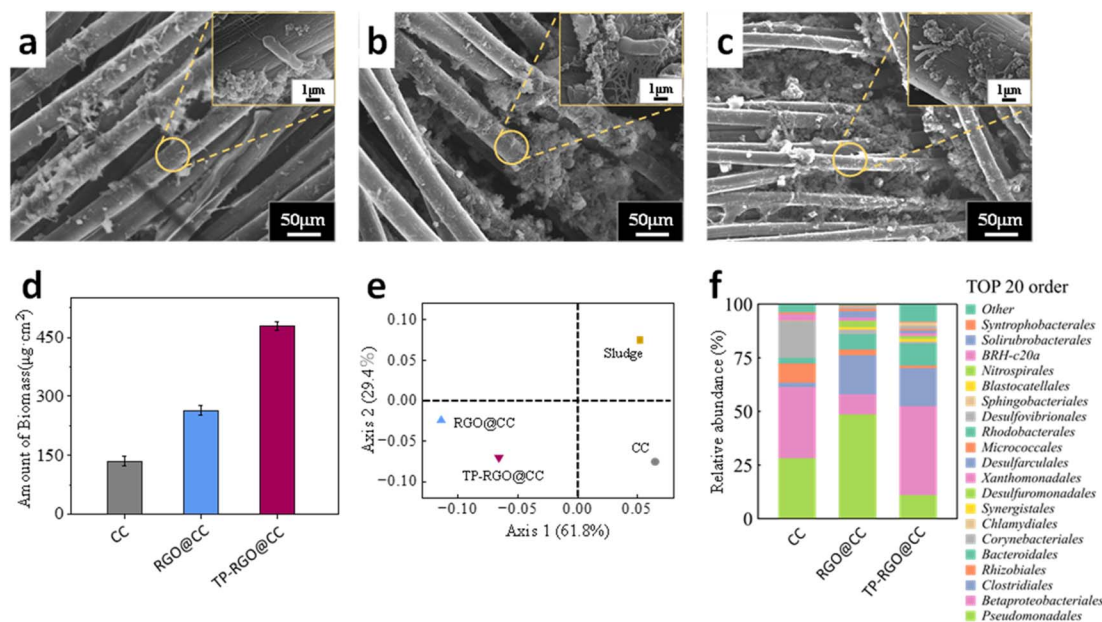

Fig. 5 SEM images of biofilm growth on (a) CC, (b) RGO@CC and (c) TP-RGO@CC anodes; (d) amount of biomass of anode; (e) principal coordinates analysis (PCoA); (f) the structure of microbial community at different anodes.

attachment on the surface of all three anodes was initially low during the early stages (1–3 days) of operation. Among them, the TP-RGO@CC anode exhibited relatively more microbial attachment on its surface and a higher number of active bacteria (green color). This phenomenon facilitated the rapid startup of the MFC electrodes, enabling them to achieve the strongest voltage. With the increase of the running time, the number of bacteria on the anode surface of different MFCs showed different degrees of increase. At the running time up to 14 days, the number of active bacteria on the surface of the RGO@CC anode increased significantly compared to that of the CC anode. Meanwhile, for the TP-RGO@CC anode, the number of active bacteria attached to the surface was significantly higher than that of the other two groups, indicating that the excellent biocompatibility of the TP-RGO@CC anode resulted in stronger microbial proliferation and vitality on the surface of the anode. This enhanced vitality provided robust support for the simultaneous power production and dye degradation ability of the MFC.

In Fig. 5e, a comprehensive view of the samples analyzed through principal coordinate analysis (PCoA) is presented, where distinct groups of samples are represented by different colored dots. The PCoA analysis reveals noteworthy changes in the microbial community structure at the modified anode, indicative of the selective pressure imposed by the modifications on microbial species. In particular, the TP-RGO@CC anode is situated farther away from the original sludge on the coordinate axis. This spatial distinction suggests that the TP-RGO@CC anode exhibits a heightened level of selectivity in shaping the microbial community, implying a more pronounced influence on the composition and distribution of microorganisms compared to other modifications.

The bacterial communities on different anodes were analyzed to delve deeper into the performance of the anode electrodes. In Fig. 5f, a histogram illustrates the species composition of loaded microorganisms on the anode at the order level after operation. For plain CC anodes, the prevalent presence of *Betaproteobacteriales*, *Pseudomonadales*, and other orders on their surfaces suggests a diverse community on the MFC anode capable of degrading a wide range of organic matter.[41,42] The MFC operating with the RGO@CC anode displayed a similar diversity but exhibited a significant increase in *Clostridiales* and *Bacteroidales*. This indicates that the RGO@CC anode possesses an enhanced capacity for organic matter degradation under anaerobic conditions.[43] *Betaproteobacteriales*, *Clostridiales*, and *Bacteroidales* dominated the TP-RGO@CC anode, emphasizing a bacterial assemblage with diverse metabolic capabilities. This diversity facilitated the efficient degradation of methyl orange dye by the MFC. In addition, on the RGO@CC and TP-RGO@CC anodes, *Desulfuromonadales* associated with extracellular electron transfer were clearly dominant, highlighting their excellent extracellular electron transfer capability.[44] This suggests that the MFC operating with the TP-RGO@CC anode can contribute to both organic matter degradation and simultaneous power production, underscoring its influence on the microbial community within the MFC.

4. Conclusion

In this work, a tea polyphenol reduced GO to modified carbon cloth electrode (TP-RGO@CC) was successfully prepared for MFC anode. The MFC with the biocompatible TP-RGO@CC anode, demonstrated an impressive power density of 773.9 mW m^{-2}. Simultaneously, it exhibited exceptional decolorization efficiency, achieving a 99% removal of methyl orange dye (50 mg L^{-1}, pH 7). The superior characteristics of the TP-RGO@CC anode surface, particularly its ability to selectively promote the growth of microorganisms, substantiate its efficacy in improving organic degradation and synchronizing electro-production mechanisms. The MFC equipped with a TP-RGO@CC anode reduces energy input while achieving environmental remediation. Meanwhile, it mitigates the toxicity of the preparation process. This aligns with the principles of green chemistry, thereby promoting environmental sustainability. Additionally, the utilization of tea dregs as a valuable biomass resource not only enhances resource efficiency but also aligns with the broader goal of promoting sustainability in natural components. These findings collectively underscore the effectiveness and potential of tea polyphenol–reduced graphene oxide anodes for dye effluent-driven MFC. The utilization of natural extracts in biocompatible anodes offers a sustainable and environmentally friendly approach to power generation and dye decolorization.

Conflicts of interest

The authors declare that they have no known competing financial interests or personal relationships that could have appeared to influence the work reported in this paper.

Acknowledgements

References

1 H. B. Slama, A. Chenari Bouket, Z. Pourhassan, F. N. Alenezi, A. Silini, H. Cherif-Silini, T. Oszako, L. Luptakova, P. Golińska and L. Belbahri, *Appl. Sci.*, 2021, **11**, 6255.

2 A. Islam, S. H. Teo, Y. H. Taufiq-Yap, C. H. Ng, D.-V. N. Vo, M. L. Ibrahim, M. M. Hasan, M. A. R. Khan, A. S. M. Nur and M. R. Awual, *Resour., Conserv. Recycl.*, 2021, **175**, 105849.

3 S. Karimifard and M. R. Alavi Moghaddam, *Sci. Total Environ.*, 2018, **640–641**, 772–797.

4 M. Ahmad, M. Yousaf, A. Nasir, I. A. Bhatti, A. Mahmood, X. Fang, X. Jian, K. Kalantar-Zadeh and N. Mahmood, *Environ. Sci. Technol.*, 2019, **53**, 2161–2170.

5 L. N. Ndlovu, K. E. Mokubung, C. Donga, N. N. Gumbi, A. K. Mishra, E. N. Nxumalo and S. B. Mishra, *J. Inorg. Organomet. Polym.*, 2023, DOI: 10.1007/s10904-023-02961-w.

6 M. Jayapal, H. Jagadeesan, M. Shanmugam, P. Danisha J and S. Murugesan, *J. Hazard. Mater.*, 2018, **354**, 231–243.

7 R. Krishnamoorthy, P. A. Jose, M. Ranjith, R. Anandham, K. Suganya, J. Prabhakaran, S. Thiyageshwari, J. Johnson, N. O. Gopal and K. Kumutha, *J. Environ. Chem. Eng.*, 2018, **6**, 588–595.

8 H. Zhang, K. Zhang, M. Gao, Z. An, C. Tang and X. Yan, *Journal of Water Process Engineering*, 2022, **50**, 103233.

9 M.-H. Cui, W.-Z. Liu, Z.-E. Tang and D. Cui, *Water Res.*, 2021, **203**, 117512.

10 N. Bazina, T. G. Ahmed, M. Almdaaf, S. Jibia and M. Sarker, *J. Biotechnol.*, 2023, **374**, 17–30.

11 E. S. Heidrich, T. P. Curtis and J. Dolfing, *Environ. Sci. Technol.*, 2011, **45**, 827–832.

12 A. Mahmoodi Nasrabadi and M. Moghimi, *J. Power Sources*, 2023, **564**, 232871.

13 J. Babauta, R. Renslow, Z. Lewandowski and H. Beyenal, *Biofouling*, 2012, **28**, 789–812.

14 T. Wilberforce, M. A. Abdelkareem, K. Elsaid, A. G. Olabi and E. T. Sayed, *Energy*, 2022, **240**, 122478.

15 G. Yildiz, M. Bolton-Warberg and F. Awaja, *Acta Biomater.*, 2021, **131**, 62–79.

16 A. M. Díez-Pascual, *Int. J. Mol. Sci.*, 2020, **21**, 3563.

17 E. T. Sayed, H. Alawadhi, A. G. Olabi, A. Jamal, M. S. Almahdi, J. Khalid and M. A. Abdelkareem, *Int. J. Hydrogen Energy*, 2021, **46**, 5975–5983.

18 L. G. Guex, B. Sacchi, K. F. Peuvot, R. L. Andersson, A. M. Pourrahimi, V. Ström, S. Farris and R. T. Olsson, *Nanoscale*, 2017, **9**, 9562–9571.

19 D. Galante, L. Banfi, G. Baruzzo, A. Basso, C. D'Arrigo, D. Lunaccio, L. Moni, R. Riva and C. Lambruschini, *Molecules*, 2019, **24**, 2636.

20 S. Raghunath, S. Budaraju, S. M. T. Gharibzahedi, M. Koubaa, S. Roohinejad and K. Mallikarjunan, *Food Eng. Rev.*, 2023, **15**, 276–308.

21 G.-Y. Tang, C.-N. Zhao, X.-Y. Xu, R.-Y. Gan, S.-Y. Cao, Q. Liu, A. Shang, Q.-Q. Mao and H.-B. Li, *Antioxidants*, 2019, **8**, 180.

22 Y. Wang, Z. Shi and J. Yin, *ACS Appl. Mater. Interfaces*, 2011, **3**, 1127–1133.

23 Y. Wang, L. Zhu and L. An, *Renewable Energy*, 2020, **162**, 2220–2226.

24 X. Xiang, Y. Zhu, M. Yin, S. Xia and C. Guo, *J. Mater. Sci.*, 2022, **57**, 3280–3294.

25 S. Miao, Y. Wei, J. Chen and X. Wei, *Crit. Rev. Food Sci. Nutr.*, 2022, 1–19.

26 I. C. Ozsefil and A. Ziylan-Yavas, *Environ. Res.*, 2023, **235**, 116703.

27 S. Verma, T. Das, V. K. Pandey and B. Verma, *Diamond Relat. Mater.*, 2022, **129**, 109361.

28 W. S. Hummers and R. E. Offeman, *J. Am. Chem. Soc.*, 1958, **80**, 1339.

29 J. Liu, Y. Feng, X. Wang, X. Shi, Q. Yang, H. Lee, Z. Zhang and N. Ren, *J. Power Sources*, 2011, **196**, 8409–8412.

30 Y. Li, J. Liu, X. Chen, X. Yuan, N. Li, W. He and Y. Feng, *Chem. Eng. J.*, 2020, **387**, 123408.

31 D. T. K. Hue, T. Shiba, Y. Maeda and N. Takenaka, *Anal. Methods*, 2017, **9**, 5797–5805.

32 Y.-N. Bai, X.-N. Wang, F. Zhang, J. Wu, W. Zhang, Y.-Z. Lu, L. Fu, T.-C. Lau and R. J. Zeng, *J. Hazard. Mater.*, 2020, **388**, 121753.

33 R. Liao, Z. Tang, Y. Lei and B. Guo, *J. Phys. Chem. C*, 2011, **115**, 20740–20746.

34 V. Milosavljevic, K. Mitrevska and V. Adam, *Sens. Actuators, B*, 2022, **353**, 131122.

35 S. Thakur and N. Karak, *Carbon*, 2012, **50**, 5331–5339.

36 Y. Yang, M. Xu, J. Guo and G. Sun, *Process Biochem.*, 2012, **47**, 1707–1714.

37 X. Yan and M.-J. Zhu, *Bioresour. Technol.*, 2023, **388**, 129764.

38 A. Chaturvedi and P. P. Kundu, *Int. J. Hydrogen Energy*, 2022, **47**, 29413–29429.

39 C. Yang, H. Luo, W. Cheng, K. Jiang, L. Lu and L. Ling, *Int. J. Environ. Sci. Technol.*, 2022, **19**, 10353–10362.

40 A. Adachi, F. E. Ouadrhiri, M. Kara, I. El Manssouri, A. Assouguem, M. H. Almutairi, R. Bayram, H. R. H. Mohamed, I. Peluso, N. Eloutassi and A. Lahkimi, *Catalysts*, 2022, **12**, 665.

41 Y. Kang, H. Sun, B. Gao, J. Dang, M. Zhang, M. Li, J. Dong, H. Wu, J. Zhang and Z. Guo, *Chem. Eng. J.*, 2022, **439**, 135742.

42 C. Wang, Y. Xing, K. Zhang, H. Zheng, Y. Zhang, X. Zhu, X. Yuan and J. Qu, *J. Power Sources*, 2023, **559**, 232625.

43 S.-J. Chen, X. Chen, B.-B. Hu, M.-Y. Wei and M.-J. Zhu, *Renewable Energy*, 2023, **211**, 166–178.

44 X. Zhang, D. Zhang, Y. Huang, K. Zhang and P. Lu, *Water Res.*, 2018, **147**, 461–471.